JOURNAL OF AIRCRAFT
Vol. 32, No. 2, March–April 1995

Pressure-Sensitive Paint Measurements on a Supersonic High-Sweep Oblique Wing Model

B. G. McLachlan,* J. H. Bell,* H. Park,† R. A. Kennelly,* J. A. Schreiner,* S. C. Smith,* and J. M. Strong‡
NASA Ames Research Center, Moffett Field, California 94035
and
J. Gallery§ and M. Gouterman¶
University of Washington, Seattle, Washington 98195

The pressure-sensitive paint method was used in the test of a high-sweep oblique wing model, conducted in the NASA Ames 9- by 7-ft Supersonic Wind Tunnel. Surface pressure data was acquired from both the luminescent paint and conventional pressure taps at Mach numbers between $M = 1.6$ and 2.0. In addition, schlieren photographs of the outer flow were used to determine the location of shock waves impinging on the model. The results show that the luminescent pressure-sensitive paint can capture both global and fine features of the static surface pressure field. Comparison with conventional pressure tap data shows good agreement between the two techniques, and that the luminescent paint data can be used to make quantitative measurements of the pressure changes over the model surface. The experiment also demonstrates the practical considerations and limitations that arise in the application of this technique under supersonic flow conditions in large-scale facilities, as well as the directions in which future research is necessary in order to make this technique a more practical wind-tunnel testing tool.

Nomenclature

A, B = paint-sensitivity coefficients
C_p = pressure coefficient
I = luminescence intensity, wind-on, grey levels
I_0 = luminescence intensity, wind-off, grey levels
M = freestream Mach number
p = surface pressure, wind-on, psia (psf, or mmHg)
p_0 = surface pressure, wind-off, psia (psf, or mmHg)
q = freestream dynamic pressure, psf
T = surface temperature, °C
x/c = airfoil chordwise coordinate, measured from leading edge, normalized with respect to chord
α = geometric angle of attack, deg
Λ = wing sweep angle, deg

Introduction

A NEW aerodynamic measurement method, pressure-sensitive paint, has recently been developed. This method employs the oxygen sensitivity of certain photoluminescent materials in the form of a "paint," in conjunction with quantitative video and image processing techniques, to map the pressure field over aerodynamic surfaces. The luminescent paint method has a number of advantages in comparison to the present conventional point measurement methods based on taps or transducers: the foremost being that it is a field measurement, air pressure at every point on the surface is sensed simultaneously, at the spatial resolution of the video camera. With a typical commercial video camera, pressure can be measured at hundreds of thousands of individual points, as opposed to the few hundred that are the practical limit of pressure taps. Furthermore, the camera can easily be adjusted to give close-up views of features of interest, something that is impossible with conventional techniques. Considerable cost savings in model construction are potentially possible since installation of large numbers of pressure taps would no longer be required. Since the requirement for large numbers of taps often reduces model strength, attainment of higher Reynolds numbers would also be possible by using a limited-instrumentation, force-only model. The pressure paint measurement system is comparable in cost to a few dozen pressure taps on a large wind-tunnel model, and the data acquisition system can be reused indefinitely, whereas taps must be installed in each new model. The cost of the luminescent paint itself is not significantly greater than that of ordinary paints.

In the U.S. the feasibility of this new approach to surface pressure measurement was first demonstrated in experiments conducted in 1989.[1-3] Since that initial feasibility demonstration other investigators have begun to successfully employ and further develop the technique.[4,5] Recently coming to light was the independent parallel development of this technology within the former Soviet Union,[6] along with its demonstration at a western European aerospace research establishment.[7] At present, the paint method has been almost exclusively employed in wind-tunnel tests, though an attempt has been made to extend the technique to flight tests.[8]

A review of the above work readily illustrates that pressure-sensitive paint technology is in its infancy. Many issues on the implementation of the method, especially in a large-scale production facility operational setting, remain open. Due to the present limited large-scale experience base, the available literature is inadequate to address the numerous questions that potential users of the method in that environment have. The purpose of this article is to make available in the open literature our experience in using the pressure-paint method in a test of a supersonic high-sweep oblique wing model conducted in the NASA Ames 9- by 7-ft Supersonic Wind Tunnel. This May 1991 test represented the first use in the U.S. of

Presented as Paper 92-2686 at the AIAA 10th Applied Aerodynamics Conference, Palo Alto, CA, June 22–24, 1992; received Aug. 3, 1992; revision received Feb. 23, 1994; accepted for publication Feb. 23, 1994.

*Research Scientist, Aerodynamics Division, M/S 227-2. Member AIAA.
†Research Scientist, Aerodynamics Division, M/S 227-2; currently Graduate Student, California Institute of Technology, Graduate Aeronautical Laboratories, Pasadena, CA. Member AIAA.
‡Test Engineer, Aerodynamics Division, M/S 227-2.
§Research Assistant, Chemistry Department.
¶Professor, Chemistry Department.

the pressure-sensitive paint under supersonic flow conditions in a production level large-scale wind-tunnel facility. This article reports the paint results of this test and specifically addresses the issues involved in the use of the pressure-sensitive paint method under compressible flow conditions in an operational environment and wind-tunnel facility typical of aircraft development testing. This description illustrates the type of data that can be produced using the paint method and their accuracy, sources of error, different approaches to data processing, and practical details of the methods implementation.

Conceptual Background

The paint method is based on the sensitivity of certain luminescent materials to the presence of molecular oxygen.[9] When a luminescent molecule absorbs a photon, it is placed in an excited energy state, from which it typically returns to the ground state by emitting a new, longer-wavelength photon. In some luminescent materials, however, free oxygen can initiate a side reaction that results in transition to the ground state occurring without a photon being emitted—a phenomenon known as oxygen quenching. For a given excitation level, the emitted light intensity varies inversely with the local oxygen partial pressure, and thus air pressure, since oxygen is a fixed mole fraction of air. Pressure-sensitive paints consist of a luminescent molecule, the sensor, dispersed in an oxygen permeable polymer binder. When this material is applied as a paint to an aerodynamic surface and irradiated with uv radiation, it becomes possible to relate the brightness of the resulting light emitted from the surface at any given point to the air pressure at that point.

The oxygen quenching of a luminescent species is usually described using the Stern-Volmer equation.[9] Although this relationship is strictly valid only for molecules in solution, experience has shown that it is an accurate description of the quenching process in the pressure-sensitive paint situation. The Stern-Volmer relation can be written in a modified form suitable for aerodynamic testing purposes[1-3] as follows:

$$(I_0/I) = A + B(p/p_0) \quad (1)$$

From Eq. (1) it is clear that operationally the paint technique requires the acquisition of luminescence intensity field images under still air (wind-off) and during airflow (wind-on) conditions. Knowledge of I_0 and I allows p to be readily calculated from Eq. (1), since p_0 is a known constant. The reason for taking the ratio of I_0 and I is that the effect of spatial nonuniformities in uv illumination intensity and coating thickness are factored out.[1] It must be noted that assumed in Eq. (1) is that the geometry of the experimental arrangement (position of uv lamps, cameras, and model) is fixed, and that uv lamp intensity is a constant.

Experimental Methods

Experimental Setup

The model, shown in Fig. 1, is a generic wing-body configuration designed to extend the data base on oblique wing aerodynamics. The wing is of slightly tapered planform, with a 14% thickness at the root decreasing linearly to 12% at 85% semispan, and has a supercritical airfoil section. The wing can be set at a variety of sweep angles from 0 to 72 deg. Chordwise rows of pressure taps were located on the top and bottom of the wing at the mid-semispan point. Each row consisted of 15 taps.

The model was sting-mounted with the plane of the wing oriented vertically, allowing top and bottom planform views through the test section side windows. For this test, the wing bottom surface was coated with the luminescent paint. Although the entire bottom surface of the wing was painted, images were only obtained of the wing's forward-swept portion due to time constraints. The top of the wing was occupied

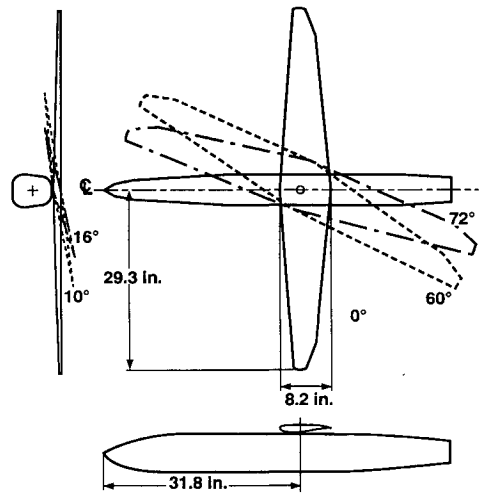

Fig. 1 Three-view scale diagram of the oblique wing model used in the test.

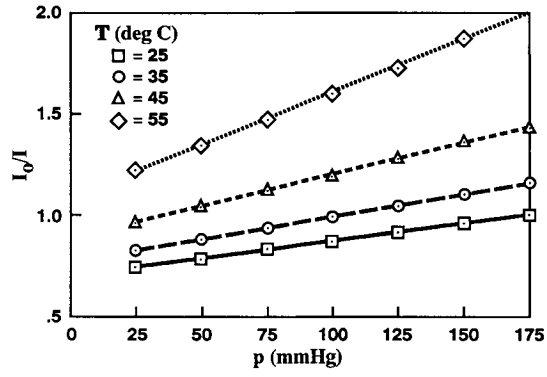

Fig. 2 Calibration curves of paint containing PtOEP on a white background at different temperatures. I_0 for each curve was measured at 25°C and 175 mmHg.

by a minitufts experiment, and the fuselage was left unpainted. Excitation of the painted surface was provided by a cluster of seven short arc mercury vapor lamps mounted at the test section side window. These 250-W lamps emit uv light in a broadband centered around 360 nm, with a cutoff filter to block emission in the visible wavelengths. The model was shielded from all other sources of illumination in order to eliminate all sources of light at the paint's emission wavelength, which would generate a spurious signal. Paint emission data were acquired with a standard RS-170 format charge-coupled-device (CCD) video camera, using an f1.4/16-mm lens, equipped with a bandpass interference filter chosen to pass only the paint's 650-nm emission wavelength. The camera was configured such that its automatic gain control was disabled and gamma = 1.0. The camera was colocated with the uv lamps. The camera output was digitized at 512 × 480 pixel spatial resolution and 8-bit grey level resolution using a frame-grabber board mounted in a personal computer. Postprocessing was performed on a graphics workstation.

Pressure-Sensitive Paint

The luminescent paint[1-3] used contained an active molecule dispersed in a polymer binder. The resulting mixture is easily applied using conventional spray painting techniques. The values of the sensitivity coefficients A and B of Eq. (1) were determined by measuring the pressure and temperature response of a representative luminescent paint sample over the range of conditions encountered in the current test. A small test plate was coated with luminescent paint and placed in a calibration chamber where the sample was exposed to a controlled pressure and temperature. The painted sample plate was exposed to uv light at the paint's 380-nm excitation wave-

Table 1 Summary of reference (wind-off) image points

Reference point	Λ, deg	Measured static press, psia	Static temperature, °C	Calculated static pressure, psia	% Difference: measured − calculated
1	72	14.74	16.7	15.25	3.5
2	72	2.70	7.2	——	——
3	72	2.73	34.4	2.67	−1.8
4	72	14.67	37.8	16.23	10.7
5	60	14.65	18.3	17.40	18.8
6	60	3.31	12.2	——	——
7	60	2.47	14.4	2.30	−6.6
8	60	2.61	39.4	2.44	−6.4
9	60	3.26	42.2	3.10	−4.7
10	60	14.65	48.9	16.82	14.8

length, and its response was measured using a CCD video camera. The emitted intensity from the paint was measured over a range of pressures from 0 to 490 psf, and temperatures from 25 to 55°C, with the results shown in Fig. 2. The data in Fig. 2 is presented in Stern-Volmer normalized form, the intensities being normalized by the intensity at a pressure of 175 mmHg, $T = 25$°C. It is evident that as temperature increases, the intensity decreases, relative intensity I_0/I increases, and relative sensitivity to pressure changes, the slope, increases. By interpolating between the curves, it is possible to determine the value of the sensitivity coefficients for a given temperature. Thus, if the surface temperature is known, the surface pressure can be calculated from the paint intensity data.

The surface to be painted was prepared by careful cleaning. A boundary-layer trip strip, normally located at the 10% chord position on the lower surface of the wing, was removed. Following the cleaning, an undercoat of a specific white enamel paint[1-3] was applied. This white undercoat acts as a scattering layer for both exciting and emitted photons, enhancing the emitted intensity of the pressure-sensitive paint. After the undercoat had been allowed to dry, the luminescent paint was applied by spraying it onto the wing with a spray gun. Careful painting technique allows some control over the roughness of the surface finish. This does not affect paint response, but can be used to alter the model's aerodynamic behavior. In this case, a rough surface was applied at approximately the same location previously occupied by the trip strip, in an attempt to ensure that the boundary-layer transition location was unchanged. During painting, the pressure taps were plugged with fine wire to avoid painting over them. An alternate procedure is to blow air through the taps during painting. Our initial experience showed, however, that this approach can lead to excessive buildup of paint in a circular mound around each tap, and so for this test the wire method was preferred. The air approach is most promising and we anticipate the difficulties will be overcome with further refinement.

Test Conditions and Data Acquisition

Data was obtained in a parametric test matrix for the following conditions: three Mach numbers ($M = 1.6$, 1.8, and 2.0), two dynamic pressures ($q = 700$ and 1000 psf), two wing sweep angles ($\Lambda = 72$ and 60 deg), and four angles of attack ($\alpha = 4$, −2, 0, and +2 deg). Predominately negative angles of attack were chosen because it was felt that the suction side would display more interesting flow phenomena resulting from the larger pressure variation across that surface. The test matrix was covered in two separate wind-tunnel runs, the first with $\Lambda = 72$ deg, followed chronologically with $\Lambda = 60$ deg. Tunnel total temperature was nominally 47 and 58°C for $q = 700$ and 1000 psf, respectively. The test matrix was chosen with the intent to explore a range of conditions that were considered fairly typical for this model and facility.

Reference, or "wind-off," images were obtained with the tunnel drive off at several different static pressures and temperatures. These are listed in Table 1 in chronological order. For each reference point, the conventionally measured static pressure at which it was taken is listed, together with the static pressure determined a priori from the paint static calibration data, and the percentage difference between the actual and calculated pressures. Images were taken for all four α values at each reference point. For each run, the procedure was to first take one set of images at atmospheric pressure, then take one or more sets of images as the tunnel was pumped down to operating pressure. After running the tunnel, the procedure was reversed. Thus reference points nos. 1, 2, 5, 6, and 7 were taken before tunnel drive start, while points nos. 3, 4, 8, 9, and 10 were taken after drive shutdown. The later points are at an elevated temperature, due to heating during tunnel operation. Wind-on data were taken in a roughly 30-min period between point nos. 2 and 3, and in a 50-min period between nos. 7 and 8. Wind-off images were taken at several different points in order to supply data for checking the paint calibration, as well as to determine which wind-off points were best-suited to ratioing the wind-on images.

Conventional pressure data were obtained from the pressure taps concurrently with the luminescent paint observations. Flow visualization of the outer flow shock structure was also acquired using the schlieren method for the same run conditions as the luminescent paint. Since the schlieren and paint techniques have incompatible illumination requirements, it was not possible to operate the systems simultaneously. It also proved instructive to compare the paint data with data obtained from several other surface flow-visualization methods that were applied to the wing during previous tests.

Image Data Reduction

The pressure signal produced by the paint is subject to several kinds of error, and some correction is required to extract pressure data from the raw images. The primary cause of difficulty arises from the need to obtain a wind-off image. Ideally, the wind-off and wind-on images should be taken close in time to one another. To accomplish this the facility must be stopped and restarted each time a new measurement is taken. This, however, is an unacceptable requirement in a large facility. In such a situation a time delay must therefore be accepted between the acquisition of the wind-on and wind-off images. As the time delay increases, a variety of effects leads to the progressive buildup of errors in the measurement. In particular, paint photodegradation and temperature sensitivity become important sources of error. An additional source of measurement error, especially important in large facilities, arises due to the movement of the model under airloads. In this situation, the wind-on and wind-off images will not be spatially aligned.

Error Sources

In practice, the uv incident intensity and paint thickness vary from point-to-point on the model surface. Figure 3 shows images taken of the oblique wing at different stages of the data reduction procedure. Figure 3a is a raw intensity field

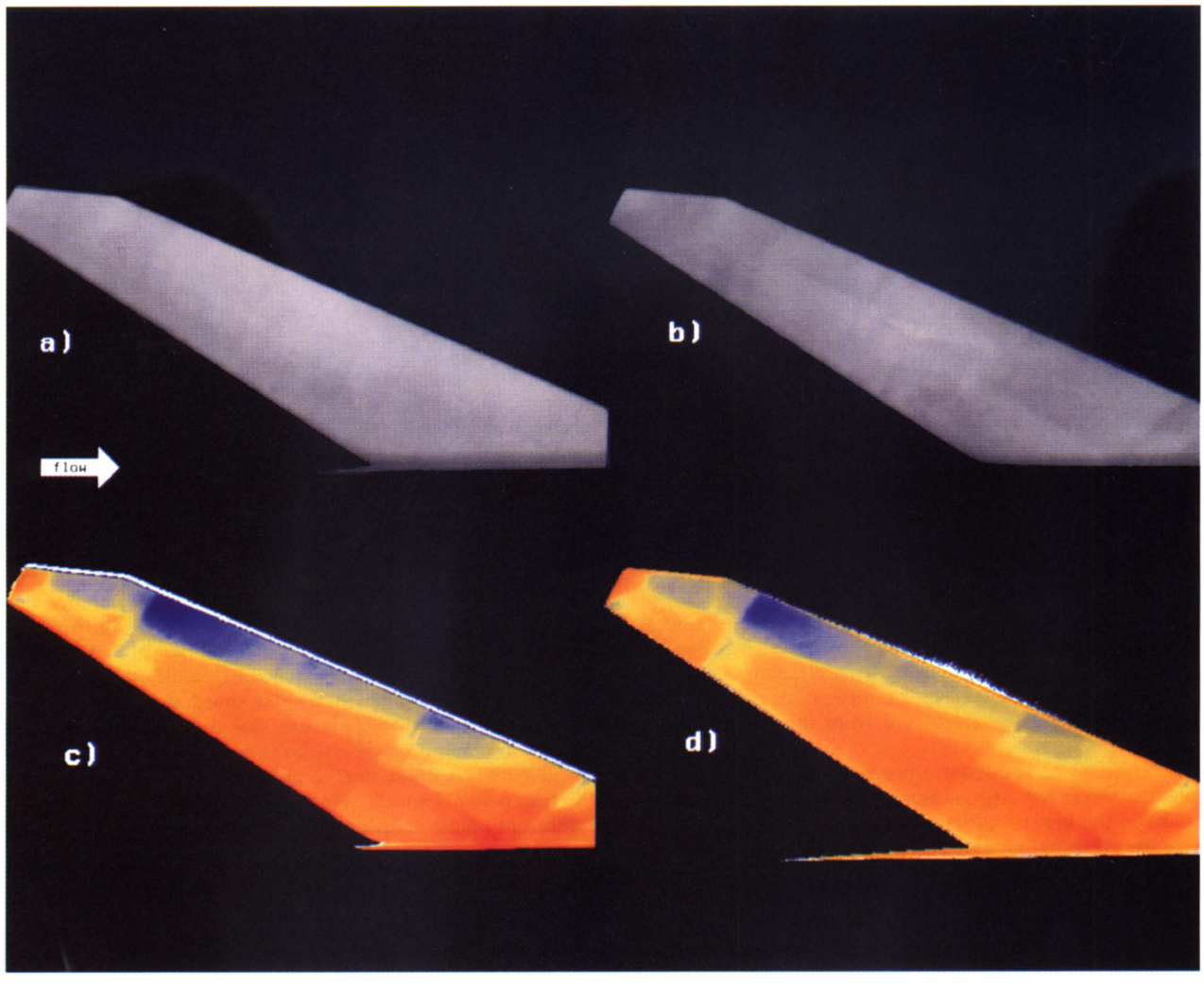

Fig. 3 Images showing steps in data reduction process: a) luminescent paint wind-off image; b) raw luminescent paint wind-on image (M = 1.6, q = 700 psf); c) ratio of image a) over image b); and d) ratio of images, with image a) registered to image b).

image with the tunnel off, and thus constant pressure over the wing surface. As is evident, the paint's brightness varies considerably from one point on the surface to another, due to spatial differences in illumination intensity, paint thickness, and model features such as panel joint lines. In Fig. 3b, the intensity field image for $M = 1.6$ is displayed. While the gross features of the pressure distribution can be discerned, fine detail is difficult to make out due to masking by the spatial nonuniformities noted above. In order to factor out these effects, we take the ratio of the two images, point-by-point, producing the image in Fig. 3c. The intensity ratio map thus produced is related to the pressure field by Eq. (1). The A and B coefficients in Eq. (1) are in general both functions of the temperature at both the wind-off and wind-on conditions. With a temperature variation being absent across the surface, however, A and B have the same value over the whole image, and once they are determined, a pressure map of the surface can be produced.

The sensitivity of the luminescent paint to pressure changes increases with increasing temperature. Even given the temperature dependence of A and B, pressure levels cannot be quantitatively determined a priori unless the temperature of the surface at each point is known as well. Thus, it would seem that the production of quantitative data from the luminescent paint would have to await the development of a means to simultaneously measure the surface temperature field. However, for many cases of practical interest this turns out not to be necessary. Often the temperature is constant over large parts of the model surface, and so coefficients determined over one portion of the surface will be applicable to the remainder of the model as well. For many transonic and low supersonic configurations, surface temperature varies only slightly within regions bounded by clearly defined shocks. If this situation exists, the Stern-Volmer coefficients can be determined by one of two methods. In the a priori method, the temperature dependence of the coefficients is first determined through separate static calibration of a paint sample in a pressure/temperature chamber. Given this data, and the temperature of a region of interest on the model surface, the appropriate values for the Stern-Volmer coefficients can be found. The alternative method, which we have termed in situ calibration, requires independent pressure measurements obtained at several points along the surface, such as a row of pressure taps. The Stern-Volmer coefficients are obtained by a least-squares fit to Eq. (1) of the measured tap pressures and paint intensities. No information about the actual surface temperature, or the temperature-dependence of the Stern-Volmer coefficients is needed, but there must be enough independent pressure data to get an accurate fit. In the present article, we will display results from both types of calibration.

The ratioing procedure introduces two sources of error into the measurement. The first occurs when the model moves between the times the wind-off and wind-on images are taken. Models installed in large facilities are typically mounted on stings that can flex several inches when the tunnel operates. In addition, the models themselves deform under airloads. Obviously, some process must be employed to "register," i.e., spatially align, the test and reference images, so that each

point on the reference image is divided by the corresponding point on the test image. The effects of registration errors can be seen by comparing Figs. 3c and 3d. In Fig. 3c, the wind-on and wind-off images have been ratioed with no attempt at spatial registration. Some amount of spurious detail is visible, especially at the edges of the wing. In Fig. 3d, the wind-on image has been spatially transformed in order to correctly match the wind-off image. The result is a considerable reduction in spurious detail. Image registration cannot completely account for model motion errors, however, since in its shifted position the model is now subject to slightly different uv illumination conditions. For small model motions this effect is negligible, and can be disregarded or corrected. For large motions, registration simply fails, and this represents a limit of the present ratioing procedure.

The second error arises due to photodegradation of the luminescent paint.[1] Exposure to uv light slowly breaks down the active molecule, reducing both the total brightness and the sensitivity to pressure variations. The rate of photodegradation increases with both increasing temperature and oxygen concentration, but decreases exponentially with exposure time. The magnitude of photodegradation can be quite severe. In the present case, it was found that the mean image brightness had decreased by a factor of two from one day to the next—the effects of this photodegradation will be discussed more fully later. Photodegradation varies linearly with the intensity of uv illumination, and so the relative decrease in brightness is the same for all parts of the image. As a result, photodegradation of the wind-on image vis-à-vis the wind-off image is factored out by the in situ calibration process described above. In contrast, the a priori calibration procedure is drastically affected by photodegradation. The Stern-Volmer coefficients determined through separate calibration have not been subject to the same photodegradation history; thus the calibration will not be accurate unless some means is used to correct for photodegradation effects, a nontrivial exercise under large-scale operational conditions.

A Priori Calibration

To perform the a priori calibration, a knowledge of the temperature dependence of the Stern-Volmer sensitivity coefficients is necessary. In the present case the data in Fig. 2 were used to determine the values of A and B at the calibration temperatures, and by interpolation at intermediate temperatures.

It was desired to compare pressure values calculated by Eq. (1) with those obtained from independent measurements. This could be done relatively easily for the reference (wind-off) conditions. Here, the tunnel air was assumed to be in equilibrium, and so the tunnel static temperature was taken to be the model surface temperature. At each reference a mean image brightness was obtained by averaging the pixel values over the wing image for all four angles of attack. One condition was then taken as the known reference condition, and Eq. (1) was used to calculate the pressure at the other conditions from the image intensity ratios. (For the 72-deg sweep angle cases, reference point 2 was used as the reference intensity, whereas for the 60-deg cases, condition 6 was used. See Table 1.) The results are shown in the "Calculated pressure" column of Table 1, with the adjacent column giving the relative difference between the measured and calculated pressure levels. The agreement between the actual and calculated values is typically within 6%, when conditions with low pressures (close to the calibration range of 0–3.4 psi) are compared. The a priori calibration is much less accurate when used to calculate conditions close to atmospheric pressure, which is outside the calibration range by a wide margin. A more extensive a priori calibration, conducted over a wider range of temperatures and pressures, is expected to lead to more accurate results.

This level of agreement between measured and calculated pressures indicates that little photodegradation has occurred

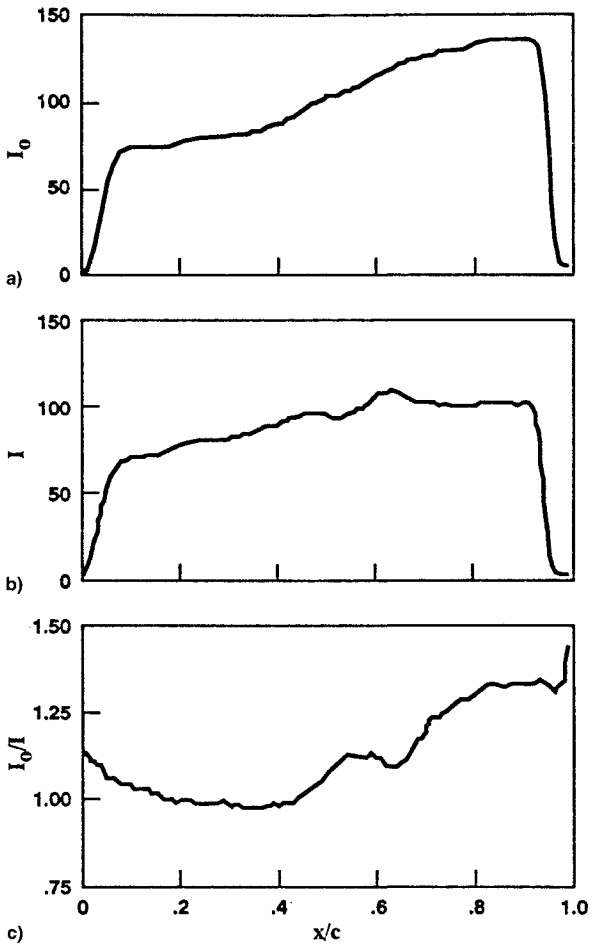

Fig. 4 Image data taken along a line parallel to the pressure taps for a representative case: a) wind-off data; b) wind-on data (M = 1.6, α = −4 deg, Λ = 60 deg, q = 700 psf); and c) ratio of curves a) and b).

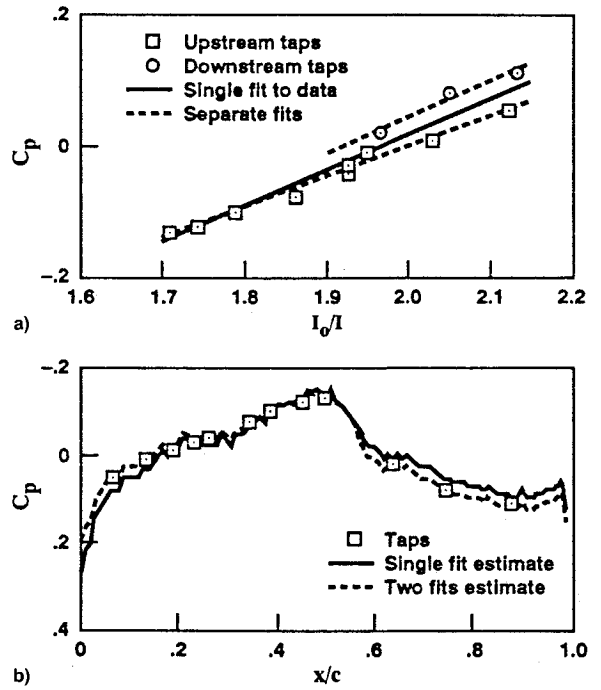

Fig. 5 Fit of luminescent paint data to pressure taps for the case where M = 1.8, α = 0 deg, Λ = 60 deg, q = 700 psf: a) curve fit of paint data to tap data and b) comparison of C_p generated by each method.

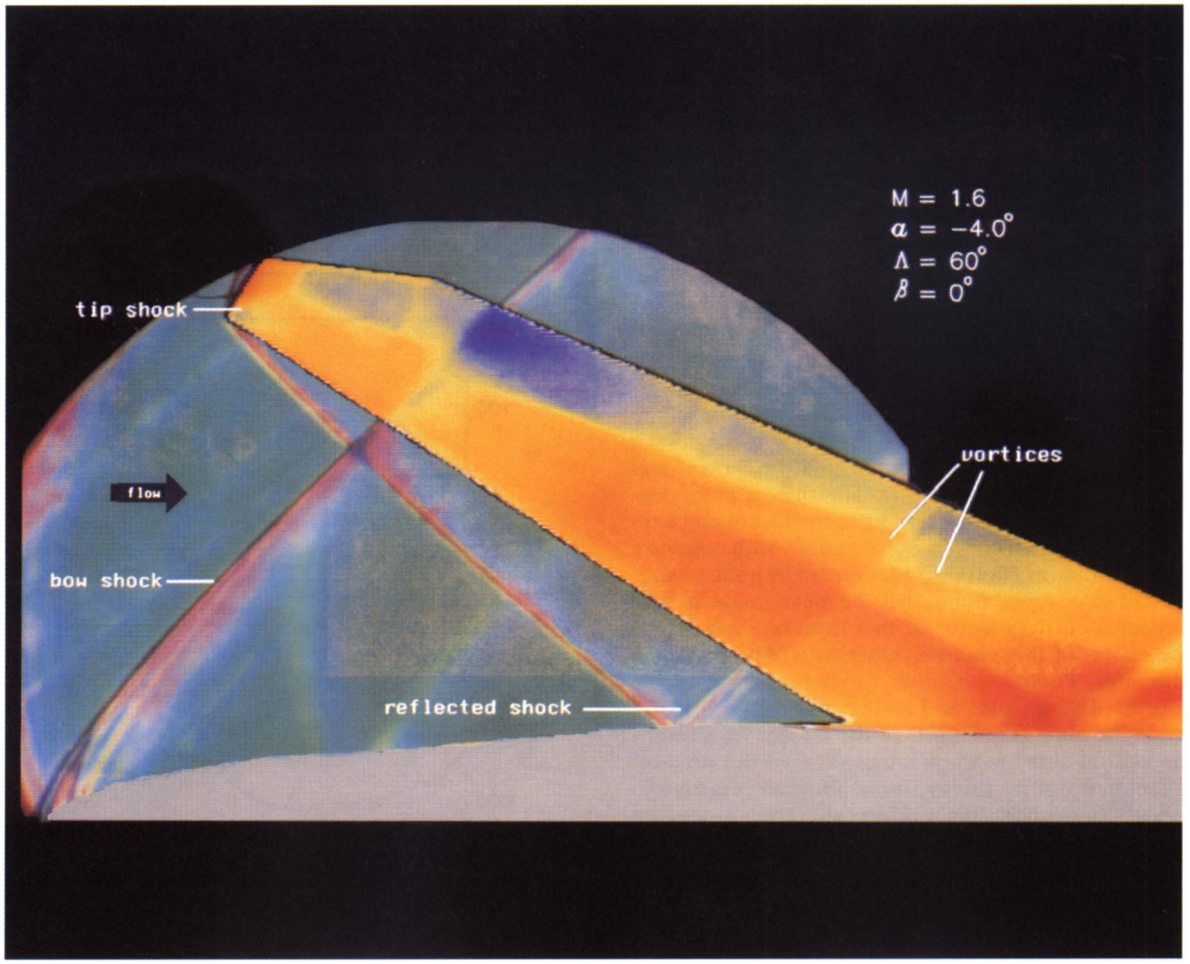

Fig. 6 Map of lower surface pressure field overlaid onto schlieren photograph. Color denotes pressure level: red is low pressure, blue is high pressure. Only forward swept wing is displayed.

between reference conditions. Photodegradation decreases image brightness, producing a calculated pressure higher than the actual pressure. Most photodegradation would be expected to occur between reference conditions nos. 2 and 3, and nos. 7 and 8, since considerable time was spent between these conditions taking wind-on data. Instead, as is clear in Table 1, the calculated pressures are lower than the measured pressures for most conditions. While the high temperatures at which the present study was conducted were expected to increase the photodegradation rate, the lowered oxygen content resulting from the low test section static pressure appears to have correspondingly reduced the photodegradation rate. This hypothesis is consistent with the relatively large positive difference in predicted and actual pressures noted at conditions 4 and 10, where the test section has been returned to atmospheric pressure while at a high temperature. Rapid photodegradation would be expected under these conditions, in which both elevated pressures and temperatures occur simultaneously.

In the present study, extensive photodegradation was noted from one day to the next. The degree of degradation can be estimated by comparing the image brightness measured at conditions 1 and 5, which were taken on consecutive days at the start of the first and second runs, respectively, and for which the pressure and temperature values are nearly identical. The brightness ratio is $I_1/I_5 = 1.77$, which is much too large to be accounted for by the slight change in the image caused by the change in wing sweep. Since the results of the a priori calibration indicate little photodegradation occurring during the run, it was concluded that most photodegradation has taken place immediately after each run, when the wing was exposed to uv light at elevated temperatures and pressures.

Attempts to extend the a priori calibration to the tunnel test conditions proved unsuccessful. The principal reason for this appears to be that the wind-on wing surface temperature is not well established. Above 35°C, the temperature variation of A and B is quite marked, putting a premium on accurate knowledge of the surface temperature. Unfortunately, the wing was not instrumented with temperature sensors, forcing an estimation of the temperature of an object whose emissivity and other thermal characteristics are not well known. Attempts to estimate the surface temperature have not resulted in an a priori calibration whose coefficients compare well with those obtained by in situ calibration, as discussed below.

In Situ Calibration

Using in situ calibration, data obtained from a conventional pressure tap was compared with intensity ratio data provided by the luminescent paint at a point close to the tap. Using data from a number of taps, the coefficients of Eq. (1) may be obtained by a simple linear fit. Since the coefficients A and B are functions only of temperature (A and B also vary with uv exposure time due to photodegradation), the resulting calibration is good over that portion of the surface that is at the same temperature as the part containing the pressure taps. In the present study, there were not expected to be any large temperature variations over the painted surface, thus making it possible to use this technique.

For calibration purposes, the tap data were compared with image data taken along a line parallel to, and just inboard of, the pressure taps. The line of image ratio data was the result of spanwise spatial averaging over five adjacent pixels. Rather than take the data from the ratioed image, raw image data from both the wind-on and wind-off images was taken, as

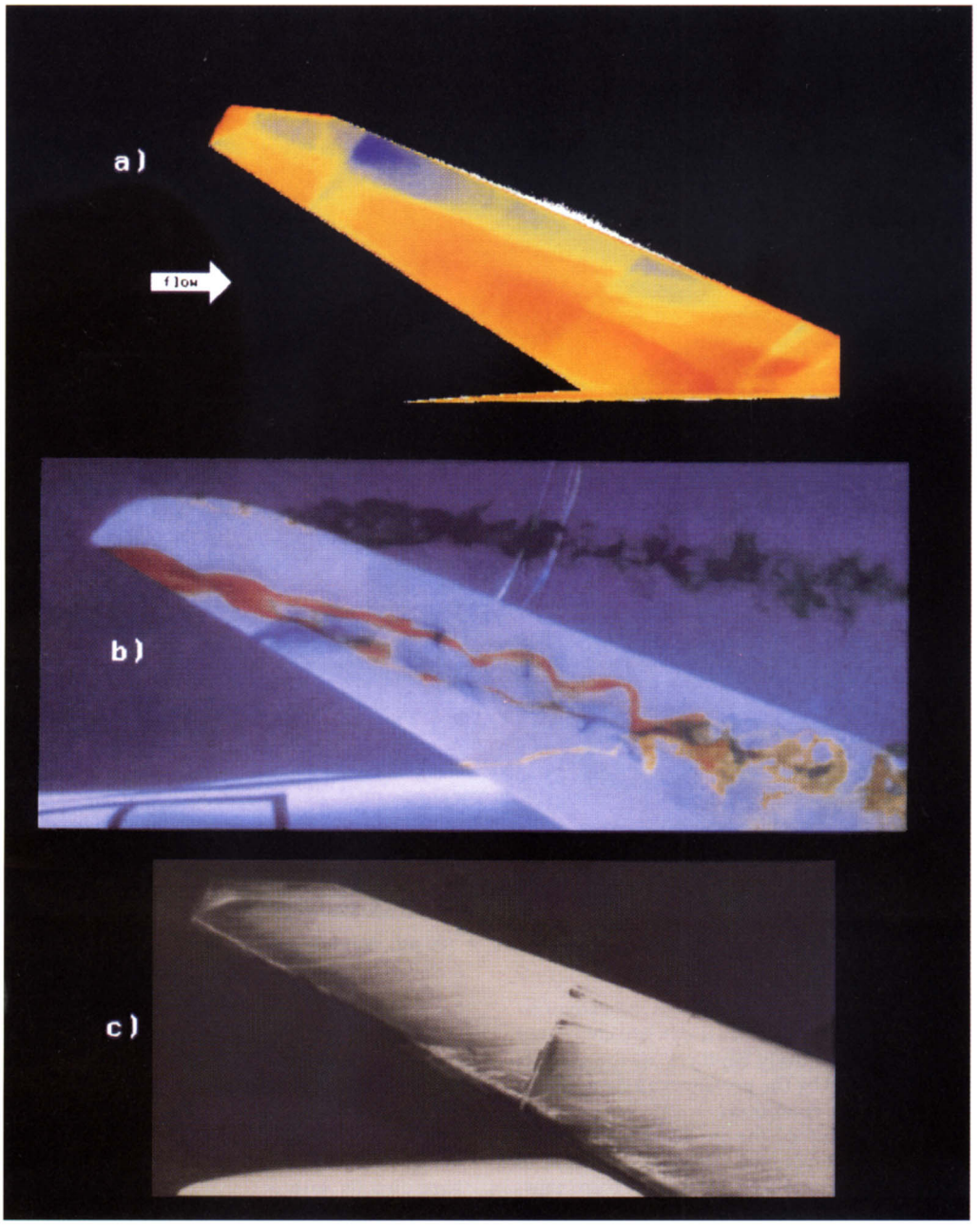

Fig. 7 Comparison of luminescent paint derived pressure data to flow visualization techniques: a) luminescent paint data at $M = 1.8$, $\alpha = -4$ deg, $\Lambda = 60$ deg, $q = 700$ psf; b) viz., water tunnel flow; and c) surface oil flow at $M = 1.6$, $\alpha = +4$ deg, $\Lambda = 68$ deg, $q = 700$ psf.

shown in Fig. 4. This was done because the values obtained from the ratioed image are subject to error depending on the degree to which the wind-on image has been registered to the wind-off image. Rather than deal with effects due to image registration, it was thought best to separate the two problems by using the raw image data directly in the calibration. In this way the registration problem is reduced to the task of lining up the two curves. This was done by establishing the location of the leading edge (defined as the point of maximum positive slope) and the trailing edge (the point of maximum negative slope) on each curve, and shifting and scaling the wind-on curve so that it matched the wind-off curve. The two curves were then ratioed, resulting in the curve shown in Fig. 4c.

Once the image ratio curve is obtained, it remains to pick out the points corresponding to the pressure tap locations. It is insufficient to simply pick points whose location in percent of chord is the same as that of the pressure taps. Perspective effects due to camera angle and the curvature of the wing produce distortions of the wing image. As a result, the tap locations in the image appear at different linear chordwise distances from the leading edge than they actually are. This distortion must be accounted for in order to relate the image data to the true geometry. In the present case, this is done by obtaining the pressure tap locations directly from the raw image. As seen in Fig. 3a, the individual pressure taps are visible as dark spots on the raw images of the wing. By looking at the raw image data along a line laid directly over the line of pressure taps, the location of each tap in the image can be determined. Once this location, as a fraction of the chord, is known, the corresponding ratioed image data can be found.

At this point the calibration procedure reduces to a least-squares fit to the Stern-Volmer equation of the image ratio data and the conventional pressure data. A representative calibration is shown in Fig. 5a, where the intensity ratio is plotted as a function of pressure coefficient for the case where $M = 1.8$, $\alpha = 0$ deg, and $\Lambda = 60$ deg. The resulting curve can be fitted relatively well with a single straight line, as illustrated by the solid line in Fig. 5a, which represents a least-squares fit to the data points. Using the coefficients determined by the fit, we plot Fig. 5b, in which the C_p data obtained

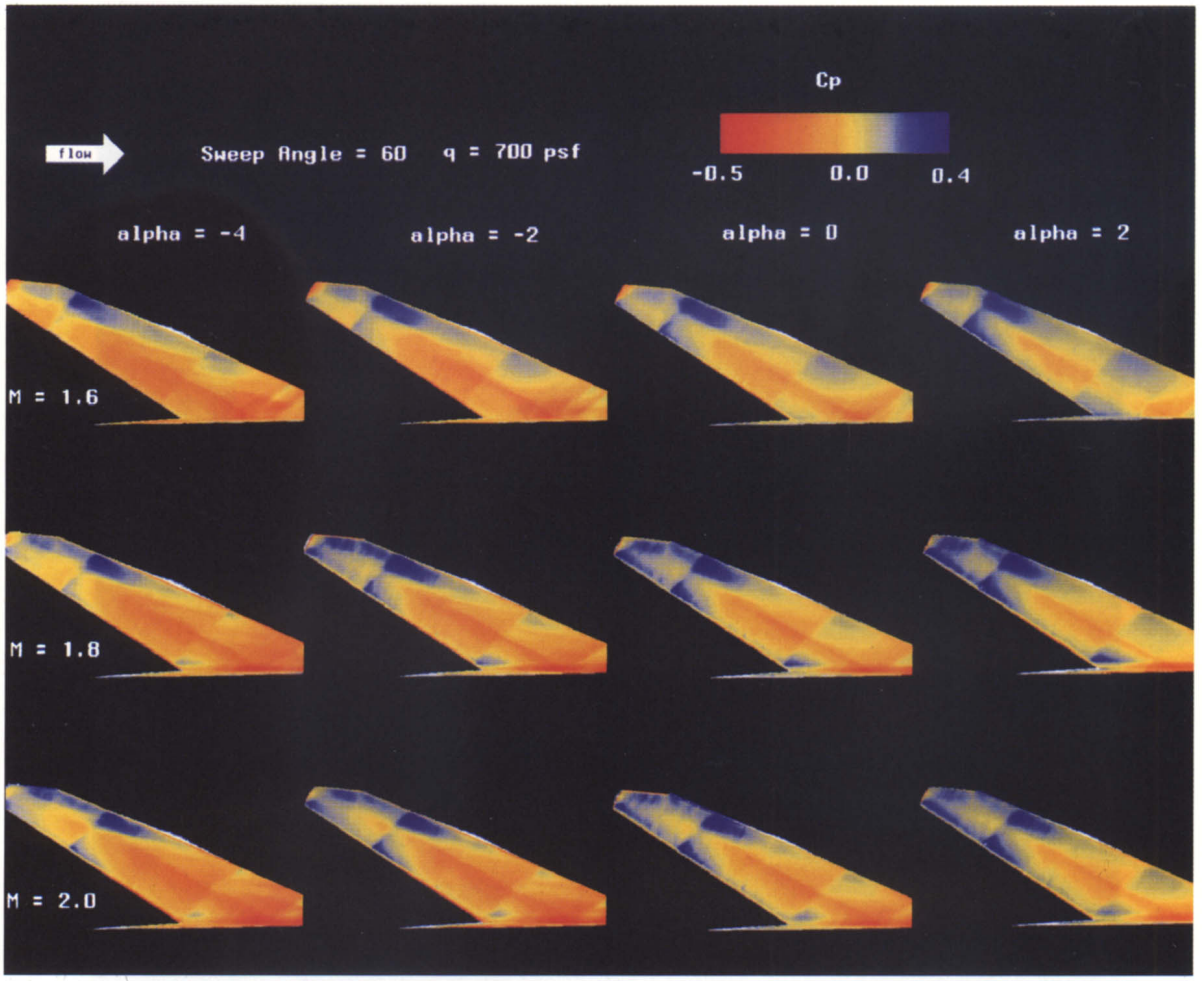

Fig. 8 Composite of oblique wing pressure maps at $\Lambda = 60$ deg, $q = 700$ psf, showing variation of surface pressure with Mach and α.

with the two methods is compared. The symbols indicate pressure tap data, while the solid line denotes the in situ calibrated paint data. The paint data faithfully captures all the characteristics of the curve described by the pressure tap data. Curve fits were obtained for all test conditions.

An estimate of the accuracy of the in situ approach was made by looking at the rms error, the standard deviation of the calculated C_p from that measured by the pressure taps. By taking the mean of the rms errors determined for each fit, we find that overall the C_p values are within 0.017 of those measured with the pressure taps. This gives an absolute accuracy of 12 psf, which is consistent with the accuracy obtained in other applications of this paint material and 8-bit resolution measurement system.

The calibration procedure described above can be improved upon. A glance at Fig. 5a shows that three of the pressure taps would be better fitted by a different straight line than that which fits the other nine taps. The three anomalous taps are those closest to the wing trailing edge, and the curve fit's steeper slope for these taps indicates that the surface temperature has increased in this region, relative to the forward part of the wing. Similar behavior was noted in a previous study of transonic flow over the suction surface of an airfoil when a shock was present on it's surface,[1-3] leading to the conclusion that an attached shock is present on the surface between the 9th and 10th tap locations for this condition. This behavior is not surprising, since the Mach number normal to the wing leading edge is 0.9, providing an aerodynamic environment conducive to shock formation. When the pressure data for each condition is separated into parts upstream and downstream of the shock, and these are fitted separately, the accuracy of the calibration is improved. The rms error of the fit to the C_p values obtained from the taps is changed to 0.011 for the upstream part and 0.015 for the downstream part. The relatively small number of pressure taps downstream of the shock makes it more difficult to obtain a good fit in this region. In addition, this multiple fitting reduced the variation in A and B from one angle of attack to the next at the same condition, which resulted when using the single curve fit procedure. This is significant, since A and B are not expected to vary directly with α.

The requirement of two fit lines to the pressure data introduces some complication into the in situ calibration process. If the calibration is to be automated, computer codes must be created that are capable of recognizing when temperature variations are occurring across the line of pressure taps, and handling this situation gracefully. Perhaps the most flexible procedure would be one in which in situ calibration is used to obtain the pressures only on that part of the model that is densely equipped with taps. Then the previously calibration chamber determined temperature dependence of the sensitivity coefficients can be used to adjust the values determined by in situ calibration to cover regions of the model where relatively few pressure taps are available.

Results and Discussion

A representative example of the luminescent paint data is shown in Fig. 6 for the case where $M = 1.6$, $\alpha = -4$ deg, $\Lambda = 60$ deg and $q = 700$ psf. The figure shows a false color map of the lower surface pressure field over the forward swept portion of the oblique wing. Color denotes pressure level: blue and red representing regions of high and low pressure, respectively. The schlieren image of the outer flow shock structure is overlaid on the surface pressure map. Note that at the condition displayed, the wing underside is imaged while at a negative angle of attack, and so the flow is characteristic

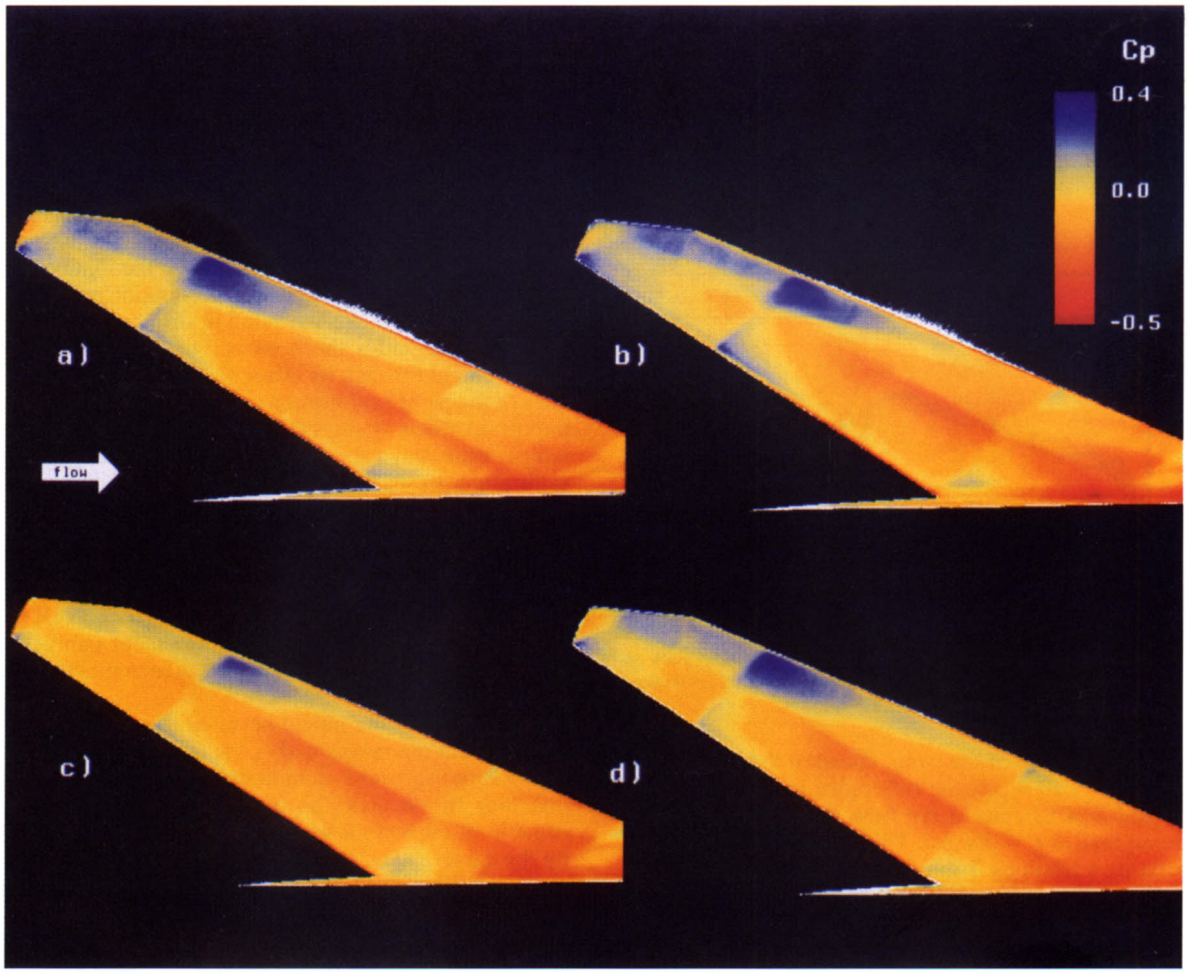

Fig. 9 Comparison of luminescent paint derived pressure data at different Mach numbers and dynamic pressures, at $\alpha = -4$ deg, $\Lambda = 60$ deg: a) $M = 1.8$, $q = 700$ psf; b) $M = 2.0$, $q = 700$ psf; c) $M = 1.8$, $q = 1000$ psf; and d) $M = 2.0$, $q = 1000$ psf.

of that over the suction surface of a highly swept supersonic wing. The unique field measurement capability of the paint is quite evident, as several features of the wing flow can be immediately discerned in the pressure map of Fig. 6. The passage of the fuselage bow shock over the outboard portion of the wing is captured, as is the passage over the inboard portion of the wing of the reflection of the wing tip shock off the fuselage. These interpretations of the luminescent paint data are corroborated by the schlieren image, which clearly shows the shock waves lining up with the pressure jumps on the wing.

More subtle features of the pressure distribution can also be recognized. Figure 7a shows the wing at $M = 1.6$, $\alpha = -4$ deg, $\Lambda = 60$ deg, $q = 700$ psf. A series of streaks running in the nominally streamwise direction can be seen on the middle portion of the wing. These streaks are regions of lower pressure induced by streamwise vortices formed over the wing surface as a result of flow separation induced by the spanwise shock. This interpretation is supported by flow visualizations of a similar model carried out in a water tunnel at the NASA Ames–Dryden Flight Research Facility. Figure 7b shows a water tunnel flow visualization of the wing upper surface at a comparable angle of attack. Flow separation at the tip generates streamwise vortices that are swept downstream along a path very similar to that seen in the luminescent paint results. Another interesting feature is the region of low pressure at the wingtip. The downstream edge of this region is denoted by a rapid pressure rise indicative of shock formation. The signature of a boundary-layer separation bubble that would accompany such a shock wave is evident in the oil-flow photograph, Fig. 7c, as a localized oil accumulation seen as a thick white line emanating from the forward corner of the wingtip. One final interesting feature that can be made out is a faint line of lower pressure flow, which is located just ahead of the bow-shock on the wing, and runs almost chordwise from the leading edge to the trailing edge at the point where the wing taper angle abruptly changes. The line of lower pressure follows a line where the wing thickness begins to decrease rapidly toward the tip. At high sweep angles, this abrupt change in thickness acts like a shoulder, and there is an expansion of the flow as it moves over this portion of the wing.

The parametric change in the pressure distribution with Mach number and angle of attack can be seen in Fig. 8, in which all the cases at $\Lambda = 60$ deg, $q = 700$ psf, are shown for each Mach number and angle of attack. This figure demonstrates the field measurement capability of luminescent paint. The variation of the different features of the pressure distribution with both Mach number and α can be seen quite readily, enhancing the overall grasp of what is going on in this complex flow.

In order to determine the effect of varying flow conditions on the performance of the luminescent paint, data were obtained for the $M = 1.8$ and 2.0 cases at two different dynamic pressures, $q = 700$ and 1000 psf. A comparison of the results is shown in Fig. 9 for the case where $\alpha = -4$ deg. While the C_p distributions should be independent of dynamic pressure (except for modest Reynolds number effects), the rise in dynamic pressure results in a corresponding rise in tunnel temperature, implying altered temperature differences across the shocks. This will result in altered paint performance due to its temperature sensitivity. While there is relatively little difference in the luminescent paint images for the $M = 2.0$ cases, some variation is visible between the $M = 1.8$ cases, especially

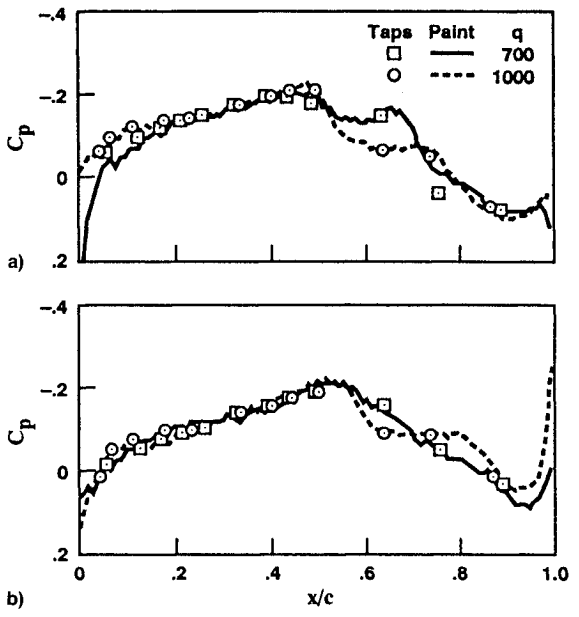

Fig. 10 Comparison of luminescent paint and pressure tap data at different Mach numbers and dynamic pressures, at $\alpha = -4$ deg, $\Lambda = 60$ deg: a) $M = 1.8$ and b) $M = 2.0$.

on the outboard section of the wing, ahead of the bow shock. At $M = 1.8$, $q = 1000$ psf, the difference in pressure levels upstream and downstream of the bow shock appears to be more intense than at $q = 700$ psf. This suggests that the effect of temperature variations is more pronounced at higher dynamic pressure. This is consistent with known luminescent paint behavior, which becomes more temperature-sensitive as the mean temperature rises. It should be noted, however, that conventional pressure measurements also show some variation as the dynamic pressure is increased. Figure 10 shows C_p plot comparisons of both the luminescent paint and pressure tap data for both Mach numbers. In each case, the luminescent paint matches the pressure tap data with good accuracy. In addition, some pressure variation occurs with Mach number, principally downstream of the spanwise shock. The variation is more pronounced for the $M = 1.8$ case.

When using the paint method the issue naturally arises as to whether the addition of the paint to the model surface alters the model's aerodynamic characteristics. An evaluation of this issue was made by comparing the chordwise pressure distribution from the pressure taps for paint-off and paint-on conditions. Negligible difference was found between the two conditions for the Mach numbers and α within the range of the current test. The paint can therefore be considered essentially nonintrusive, at least for the model geometry of the present test. A definitive answer on this issue will have to await the gathering of a broader experience base with this technology.

Concluding Remarks

The present results show both the usefulness of the luminescent pressure-sensitive paint method and the need for further research. Currently, this technique allows the experimenter to quickly and inexpensively measure the mean surface pressure field over a wind-tunnel model. Even from a qualitative standpoint, this information can be quite useful. Regions of special interest can be identified, and relative pressure levels can be determined at a glance. With a relatively small number of pressure taps on the model, the luminescent paint data can be calibrated to give quantitative pressure measurements. In the present investigation, luminescent paint data could be fit to pressure tap data to an accuracy of 12 psf, or a C_p variation of 0.017. If pressure taps are not present, a less accurate calibration may still be achievable by using a priori techniques that exploit the known response characteristics of the paint. A priori calibrations for this test were accurate to within 6–10% when surface temperature was known.

Another useful result was the discovery that photodegradation need not be a major problem in large-scale facilities. The NASA Ames 9- by 7-ft Supersonic Tunnel, in particular, is typically run at static pressures so low that photodegradation during runs is negligible, despite the high total temperature.

This test has also illustrated some of the practical considerations and limitations that arise when the luminescent pressure-sensitive paint is employed to obtain quantitative data in large-scale facilities. Variation in surface temperature over the model degrades the accuracy of the luminescent paint measurement through its effect on the experimenter's knowledge of the paint's calibration characteristics. This is especially important when in situ calibration is used, since the surface temperature may vary over the locations of the taps used for calibration. Research is underway to develop luminescent materials with a lower temperature sensitivity, as well as on ways to correct the pressure data, given independent measurements of the surface temperature. One promising means of obtaining temperature data is through techniques that provide a measurement over the entire model surface, such as IR thermography or temperature-sensitive luminescent paints,[10] both of which offer the possibility of simultaneous pressure and temperature field measurements.

The motion of the model between the acquisition of wind-off and wind-on images makes the use of some form of image registration software mandatory. In addition to spatially matching the images, the registration software needs to be capable of correcting for perspective distortions introduced by the camera viewing angle in order to accurately match-up corresponding parts of the luminescent paint images. The problem of registration for luminescent paint images forms a subset of the general image registration problem more typically encountered in mapping from aerial photographs and synthetic aperture radar (SAR) imagery. In addition to the problem of registering two-dimensional images, there is also the possibility of mapping luminescent paint images onto a three-dimensional representation of the wind-tunnel model. This will be necessary if it is desired to integrate the surface pressure data so as to calculate the forces and moments on the model. Image registration is by far the most computationally intensive part of the data reduction process for the luminescent paint method, and our research on this topic is continuing.

In the long term, luminescent paint techniques have the potential to greatly increase the speed and efficiency of large-scale wind-tunnel testing. Using both pressure- and temperature-sensitive paints, and imaging the model from several angles, the pressure and temperature fields over the entire surface could be obtained. Data reduction procedures requiring only a few seconds of computer time would give sufficient accuracy to allow wind-tunnel experimenters to choose the flow conditions of greatest interest during the run itself, optimizing the use of the tunnel. Within a few hours, accurate pressure and temperature fields could be reconstructed and mapped onto a three-dimensional representation of the model, thus allowing force and moment data to be computed. Without the need for large numbers of pressure taps, wind-tunnel models could be constructed faster and less expensively. In short, the widespread use of a reliable luminescent paint system could lead to a significant reduction in the cycle times currently associated with aircraft development wind-tunnel testing.

Acknowledgments

We thank the Ames Basic Research Council, in particular former heads D. Cooper and W. Warmbrodt, whose support made this work possible; R. Presley, for providing an atmosphere conducive to this work; J. Del Frate for providing the water tunnel flow-visualization results; and M. Tobak, for

enlightening discussions on oblique wing aerodynamic phenomena.

References

[1]McLachlan, B. G., Kavandi, J. L., Callis, J. B., Gouterman, M., Green, D., Khalil, G., and Burns, D., "Surface Pressure Field Mapping Using Luminescent Coatings," *Experiments in Fluids*, Vol. 14, No. 1/2, 1993, pp. 33–41.

[2]Kavandi, J. L., "Luminescence Imaging for Aerodynamic Pressure Measurements," Ph.D. Dissertation, Chemistry Dept., Univ. of Washington, Seattle, WA, 1990.

[3]Kavandi, J., Callis, J., Gouterman, M., Khalil, G., Wright, D., Green, E., Burns, D., and McLachlan, B., "Luminescent Barometry in Wind Tunnels," *Review of Scientific Instruments*, Vol. 61, No. 5, 1990, pp. 3340–3347.

[4]Morris, M. J., Donovan, J. F., Kegelman, J. T., Schwab, S. D., Levy, R. L., and Crites, R. C., "Aerodynamic Applications of Pressure-Sensitive Paint," AIAA Paper 92-0264, Jan. 1992.

[5]Crites, R. C., Benne, M. E., Morris, M. J., and Donovan, J. F., "Optical Surface Pressure Measurement: Initial Experience in the MCAIR PSTWT," *Proceedings of the Wind Tunnels and Wind Tunnel Test Techniques Conference*, Royal Aeronautical Society, London, 1992, pp. 9.1–9.13.

[6]Volan, A., and Alati, L., "A New Optical Pressure Measurement System," *Proceedings of the 14th International Congress on Instrumentation in Aerospace Simulation Facilities (ICIASF)*, Inst. of Electrical and Electronics Engineers, New York, 1991, pp. 10–16.

[7]Engler, R. H., Hartmann, K., and Schulze, B., "Aerodynamic Assessment of an Optical Pressure Measurement System (OPMS) by Comparison with Conventional Pressure Measurements in a High Speed Wind Tunnel," *Proceedings of the 14th International Congress on Instrumentation in Aerospace Simulation Facilities (ICIASF)*, Inst. of Electrical and Electronics Engineers, New York, 1991, pp. 17–24.

[8]McLachlan, B. G., Bell, J. H., Espina, J., Gallery, J., Gouterman, M., Demandante, C. G. N., and Bjarke, L., "Flight Testing of a Luminescent Surface Pressure Sensor," NASA TM-103970, Oct. 1992.

[9]Parker, C. A., "Photoluminescence of Solutions," 1st ed., Elsevier, Amsterdam, 1968, pp. 69–127, Chap. 2.

[10]Gallery, J. Gouterman, M., Callis, J., Khalil, G., McLachlan, B. G., and Bell, J. H., "Aerodynamic Temperature Measurements by Luminescence Imaging," *Review of Scientific Instruments*, Vol. 65, No. 3, 1994, pp. 712–720.